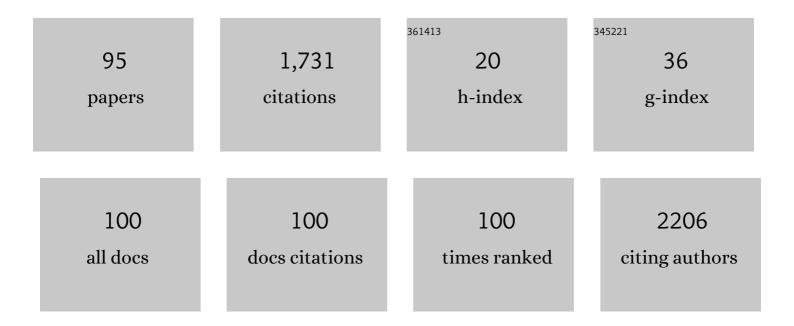
Nam-Chul Ha

List of Publications by Year in descending order

Source: https://exaly.com/author-pdf/9485879/publications.pdf Version: 2024-02-01



Ναμα-Ομιμ Ηα

#	Article	IF	CITATIONS
1	Structure of the plant growth-promoting factor YxaL from the rhizobacterium <i>Bacillus velezensis</i> and its application to protein engineering. Acta Crystallographica Section D: Structural Biology, 2022, 78, 104-112.	2.3	0
2	A pGpG-specific phosphodiesterase regulates cyclic di-GMP signaling in Vibrio cholerae. Journal of Biological Chemistry, 2022, 298, 101626.	3.4	10
3	Crystal structure of progeria mutant S143F lamin A/C reveals increased hydrophobicity driving nuclear deformation. Communications Biology, 2022, 5, 267.	4.4	3
4	Crystal structures of YeiE from <i>Cronobacter sakazakii</i> and the role of sulfite tolerance in gram-negative bacteria. Proceedings of the National Academy of Sciences of the United States of America, 2022, 119, e2118002119.	7.1	6
5	Crystal structure of the domain-swapped dimeric maltodextrin-binding protein MalE from <i>Salmonella enterica</i> . Acta Crystallographica Section D: Structural Biology, 2022, 78, 613-622.	2.3	2
6	NADH-dependent butanol dehydrogenase from <i>Fusobacterium nucleatum</i> : purification, crystallization, and X-ray crystallographic analysis. Biodesign, 2022, 10, 29-33.	0.4	1
7	Cyclin-dependent kinase 1 depolymerizes nuclear lamin filaments by disrupting the head-to-tail interaction of the lamin central rod domain. Journal of Biological Chemistry, 2022, 298, 102256.	3.4	6
8	Design and evaluation of IKK-activated GSK3β inhibitory peptide as an inflammation-responsive anti-colitic therapeutic. Biomaterials Science, 2021, 9, 6584-6596.	5.4	3
9	Progerinin, an optimized progerin-lamin A binding inhibitor, ameliorates premature senescence phenotypes of Hutchinson-Gilford progeria syndrome. Communications Biology, 2021, 4, 5.	4.4	23
10	Substrate-dependent effects of quaternary structure on RNase E activity. Genes and Development, 2021, 35, 286-299.	5.9	9
11	The flavonoid morin alleviates nuclear deformation in aged cells by disrupting progerin-lamin A/C binding. Journal of Functional Foods, 2021, 77, 104331.	3.4	2
12	Purification, crystallization, and preliminary X-ray analysis of a putative N-terminal acetyltransferase encoded by a Salmonellainfecting bacteriophage. Biodesign, 2021, 9, 19-22.	0.4	1
13	Beta-strand-mediated dimeric formation of the Ig-like domains of human lamin A/C and B1. Biochemical and Biophysical Research Communications, 2021, 550, 191-196.	2.1	8
14	Crystal structure of the nuclease and capping domain of SbcD from Staphylococcus aureus. Journal of Microbiology, 2021, 59, 584-589.	2.8	0
15	Human WRN is an intrinsic inhibitor of progerin, abnormal splicing product of lamin A. Scientific Reports, 2021, 11, 9122.	3.3	4
16	Epigallocatechin Gallate Inhibits the Uridylate-Specific Endoribonuclease Nsp15 and Efficiently Neutralizes the SARS-CoV-2 Strain. Journal of Agricultural and Food Chemistry, 2021, 69, 5948-5954.	5.2	54
17	Purification and preliminary X-ray analysis of YbeY from Staphylococcus aureus. Biodesign, 2021, 9, 41-45.	0.4	0
18	Structure and Function of the Autolysin SagA in the Type IV Secretion System of Brucella abortus. Molecules and Cells, 2021, 44, 517-528.	2.6	4

Nam-Chul Ha

#	Article	IF	CITATIONS
19	Separation of Coiled-Coil Structures in Lamin A/C Is Required for the Elongation of the Filament. Cells, 2021, 10, 55.	4.1	10
20	Novel chemical inhibitor against SOD1 misfolding and aggregation protects neuron-loss and ameliorates disease symptoms in ALS mouse model. Communications Biology, 2021, 4, 1397.	4.4	8
21	High-resolution structures of annexin A5 in a two-dimensional array. Journal of Structural Biology, 2020, 209, 107401.	2.8	6
22	Acetylation of UHRF1 Regulates Hemi-methylated DNA Binding and Maintenance of Genome-wide DNA Methylation. Cell Reports, 2020, 32, 107958.	6.4	9
23	Structure and function of the hypochlorous acid–induced flavoprotein RclA from Escherichia coli. Journal of Biological Chemistry, 2020, 295, 3202-3212.	3.4	18
24	BH4 activates CaMKK2 and rescues the cardiomyopathic phenotype in rodent models of diabetes. Life Science Alliance, 2020, 3, e201900619.	2.8	10
25	Purification, crystallization, and preliminary analysis of the lysozyme-like enzyme SagA from Brucella abortus. Biodesign, 2020, 8, 64-67.	0.4	1
26	Real-Time Measurement of the Liquid Amount in Cryo-Electron Microscopy Grids Using Laser Diffraction of Regular 2-D Holes of the Grids. Molecules and Cells, 2020, 43, 298-303.	2.6	2
27	Cleavage-Dependent Activation of ATP-Dependent Protease HslUV from. Molecules and Cells, 2020, 43, 694-704.	2.6	3
28	Tetrahydrobiopterin enhances mitochondrial biogenesis and cardiac contractility via stimulation of PGC11± signaling. Biochimica Et Biophysica Acta - Molecular Basis of Disease, 2019, 1865, 165524.	3.8	12
29	Structural basis for lamin assembly at the molecular level. Nature Communications, 2019, 10, 3757.	12.8	73
30	Crystal Structure of <i>Aeromonas hydrophila</i> Cytoplasmic 5′-Methylthioadenosine/ <i>S</i> -Adenosylhomocysteine Nucleosidase. Biochemistry, 2019, 58, 3136-3143.	2.5	0
31	Structural insight into the carboxylesterase BioH from Klebsiella pneumoniae. Biochemical and Biophysical Research Communications, 2019, 520, 538-543.	2.1	5
32	Crystal structure of the Siderophore-interacting protein SIP from Aeromonas hydrophila. Biochemical and Biophysical Research Communications, 2019, 519, 23-28.	2.1	2
33	Structural insight of the 5-(Hydroxyethyl)-methylthiazole kinase ThiM involving vitamin B1 biosynthetic pathway from the Klebsiella pneumoniae. Biochemical and Biophysical Research Communications, 2019, 518, 513-518.	2.1	3
34	Structural and functional analyses of the lipase CinB from Enterobacter asburiae. Biochemical and Biophysical Research Communications, 2019, 519, 274-279.	2.1	4
35	Biochemical and structural analysis of the Klebsiella pneumoniae cytidine deaminase CDA. Biochemical and Biophysical Research Communications, 2019, 519, 280-286.	2.1	5
36	Transcriptomic Identification and Biochemical Characterization of HmpA, a Nitric Oxide Dioxygenase, Essential for Pathogenesis of Vibrio vulnificus. Frontiers in Microbiology, 2019, 10, 2208.	3.5	9

#	Article	IF	CITATIONS
37	Plant growth-promoting activity of beta-propeller protein YxaL secreted from Bacillus velezensis strain GH1-13. PLoS ONE, 2019, 14, e0207968.	2.5	16
38	Recent paradigm shift in the assembly of bacterial tripartite efflux pumps and the type I secretion system. Journal of Microbiology, 2019, 57, 185-194.	2.8	8
39	Small-molecule inhibitor of HlyU attenuates virulence of Vibrio species. Scientific Reports, 2019, 9, 4346.	3.3	19
40	p53 induces senescence through Lamin A/C stabilization-mediated nuclear deformation. Cell Death and Disease, 2019, 10, 107.	6.3	22
41	Structural basis for HOCl recognition and regulation mechanisms of HypT, a hypochlorite-specific transcriptional regulator. Proceedings of the National Academy of Sciences of the United States of America, 2019, 116, 3740-3745.	7.1	26
42	Crystal Structure of Bacterial Cystathionine Γ-Lyase in The Cysteine Biosynthesis Pathway of Staphylococcus aureus. Crystals, 2019, 9, 656.	2.2	11
43	The coordinated action of RNase III and RNase G controls enolase expression in response to oxygen availability in Escherichia coli. Scientific Reports, 2019, 9, 17257.	3.3	8
44	LysPBC2, a Novel Endolysin Harboring a Bacillus cereus Spore Binding Domain. Applied and Environmental Microbiology, 2019, 85, .	3.1	27
45	Crystal Structure of SAV0927 and Its Functional Implications. Journal of Microbiology and Biotechnology, 2019, 29, 500-505.	2.1	1
46	Crystal Structure of LysB4, an Endolysin from -Targeting Bacteriophage B4. Molecules and Cells, 2019, 42, 79-86.	2.6	4
47	Structural insights into the apo-structure of Cpf1 protein from Francisella novicida. Biochemical and Biophysical Research Communications, 2018, 498, 775-781.	2.1	6
48	Structural and Biochemical Analysis of the Citrate-Responsive Mechanism of the Regulatory Domain of Catabolite Control Protein E from <i>Staphylococcus aureus</i> . Biochemistry, 2018, 57, 6054-6060.	2.5	5
49	Crystal structure of GSK3β in complex with the flavonoid, morin. Biochemical and Biophysical Research Communications, 2018, 504, 519-524.	2.1	18
50	Structure-based protein engineering of bacterial β-xylosidase to increase the production yield of xylobiose from xylose. Biochemical and Biophysical Research Communications, 2018, 501, 703-710.	2.1	17
51	Pharmacologic inhibition of AKT leads to cell death in relapsed multiple myeloma. Cancer Letters, 2018, 432, 205-215.	7.2	4
52	KDM2B is a histone H3K79 demethylase and induces transcriptional repression <i>via</i> sirtuinâ€1â€mediated chromatin silencing. FASEB Journal, 2018, 32, 5737-5750.	0.5	67
53	Crystal structure of E.Âcoli ZinT with one zinc-binding mode and complexed with citrate. Biochemical and Biophysical Research Communications, 2018, 500, 139-144.	2.1	8
54	Crystal structure of the nicotinamidase/pyrazinamidase PncA from Bacillus subtilis. Biochemical and Biophysical Research Communications, 2018, 503, 2906-2911.	2.1	4

#	Article	IF	CITATIONS
55	Crystal structure of peroxiredoxin 3 from <i>>Vibrio vulnificus</i> and its implications for scavenging peroxides and nitric oxide. IUCrJ, 2018, 5, 82-92.	2.2	10
56	A Novel Tetrameric Assembly Configuration in VV2_1132, a LysR-Type Transcriptional Regulator in. Molecules and Cells, 2018, 41, 301-310.	2.6	9
57	The hydrogen peroxide hypersensitivity of OxyR2 in Vibrio vulnificus depends on conformational constraints. Journal of Biological Chemistry, 2017, 292, 7223-7232.	3.4	14
58	Structural basis for the transglycosylase activity of a GH57-type glycogen branching enzyme from Pyrococcus horikoshii. Biochemical and Biophysical Research Communications, 2017, 484, 850-856.	2.1	28
59	Crystal structure of Streptomyces coelicolor RraAS2, an unusual member of the RNase E inhibitor RraA protein family. Journal of Microbiology, 2017, 55, 388-395.	2.8	5
60	Stoichiometry and mechanistic implications of the MacAB-TolC tripartite efflux pump. Biochemical and Biophysical Research Communications, 2017, 494, 668-673.	2.1	10
61	Hexameric assembly of membrane fusion protein YknX of the sporulation delaying efflux pump from Bacillus amyloliquefaciens. Biochemical and Biophysical Research Communications, 2017, 493, 152-157.	2.1	6
62	Structural and Functional Analyses of Periplasmic 5′-Methylthioadenosine/ <i>S</i> -Adenosylhomocysteine Nucleosidase from <i>Aeromonas hydrophila</i> . Biochemistry, 2017, 56, 5347-5355.	2.5	5
63	Functional implications of hexameric assembly of RraA proteins from Vibrio vulnificus. PLoS ONE, 2017, 12, e0190064.	2.5	5
64	Crystal Structure of the Regulatory Domain of AphB from Vibrio vulnificus, a Virulence Gene Regulator. Molecules and Cells, 2017, 40, 299-306.	2.6	21
65	Anti-cancer effect of novel PAK1 inhibitor via induction of PUMA-mediated cell death and p21-mediated cell cycle arrest. Oncotarget, 2017, 8, 23690-23701.	1.8	12
66	Crystal Structure of a Soluble Fragment of the Membrane Fusion Protein HlyD in a Type I Secretion System of Gram-Negative Bacteria. Structure, 2016, 24, 477-485.	3.3	49
67	RraAS2 requires both scaffold domains of RNase ES for high-affinity binding and inhibitory action on the ribonucleolytic activity. Journal of Microbiology, 2016, 54, 660-666.	2.8	8
68	Crystal structures of the disulfide reductase DsbM from <i>Pseudomonas aeruginosa</i> . Acta Crystallographica Section D: Structural Biology, 2016, 72, 1100-1109.	2.3	6
69	OxyR2 Functions as a Three-state Redox Switch to Tightly Regulate Production of Prx2, a Peroxiredoxin of Vibrio vulnificus. Journal of Biological Chemistry, 2016, 291, 16038-16047.	3.4	11
70	Crystal structure and functional implications of the tandem-type universal stress protein UspE from Escherichia coli. BMC Structural Biology, 2016, 16, 3.	2.3	6
71	Inhibiting DX2-p14/ARF Interaction Exerts Antitumor Effects in Lung Cancer and Delays Tumor Progression. Cancer Research, 2016, 76, 4791-4804.	0.9	28
72	Pseudoatomic Structure of the Tripartite Multidrug Efflux Pump AcrAB-TolC Reveals the Intermeshing Cogwheel-like Interaction between AcrA and TolC. Structure, 2016, 24, 272-276.	3.3	49

#	Article	IF	CITATIONS
73	The Crystal Structure of the YknZ Extracellular Domain of ABC Transporter YknWXYZ from Bacillus amyloliquefaciens. PLoS ONE, 2016, 11, e0155846.	2.5	17
74	Molecular architecture of the bacterial tripartite multidrug efflux pump focusing on the adaptor bridging model. Journal of Microbiology, 2015, 53, 355-364.	2.8	12
75	Structure of the Tripartite Multidrug Efflux Pump AcrAB-TolC Suggests an Alternative Assembly Mode. Molecules and Cells, 2015, 38, 180-186.	2.6	67
76	Structural details of the OxyR peroxide-sensing mechanism. Proceedings of the National Academy of Sciences of the United States of America, 2015, 112, 6443-6448.	7.1	122
77	MdsABC-Mediated Pathway for Pathogenicity in Salmonella enterica Serovar Typhimurium. Infection and Immunity, 2015, 83, 4266-4276.	2.2	15
78	Structural and Mechanistic Insights into the Pseudomonas fluorescens 2-Nitrobenzoate 2-Nitroreductase NbaA. Applied and Environmental Microbiology, 2015, 81, 5266-5277.	3.1	3
79	Crystal structure of β-N-acetylglucosaminidase CbsA from Thermotoga neapolitana. Biochemical and Biophysical Research Communications, 2015, 464, 869-874.	2.1	5
80	Crystal Structure of DsbA from Corynebacterium diphtheriae and Its Functional Implications for CueP in Gram-Positive Bacteria. Molecules and Cells, 2015, 38, 715-722.	2.6	7
81	Interaction Mediated by the Putative Tip Regions of MdsA and MdsC in the Formation of a Salmonella-Specific Tripartite Efflux Pump. PLoS ONE, 2014, 9, e100881.	2.5	17
82	Structure of a DsbF homologue from <i>Corynebacterium diphtheriae</i> . Acta Crystallographica Section F, Structural Biology Communications, 2014, 70, 1167-1172.	0.8	3
83	Periplasmic disulfide isomerase DsbC is involved in the reduction of copper binding protein CueP from Salmonella enterica serovar Typhimurium. Biochemical and Biophysical Research Communications, 2014, 446, 971-976.	2.1	12
84	Gold nanoparticle–DNA aptamer composites as a universal carrier for in vivo delivery of biologically functional proteins. Journal of Controlled Release, 2014, 196, 287-294.	9.9	48
85	Development of Akt-activated GSK3Î ² inhibitory peptide. Biochemical and Biophysical Research Communications, 2013, 434, 735-739.	2.1	12
86	Structural Basis for the Inhibition of Human Lysozyme by PliC from <i>Brucella abortus</i> . Biochemistry, 2013, 52, 9385-9393.	2.5	16
87	Morin attenuates tau hyperphosphorylation by inhibiting GSK3β. Neurobiology of Disease, 2011, 44, 223-230.	4.4	87
88	Upregulation of RNase E activity by mutation of a site that uncompetitively interferes with RNA binding. RNA Biology, 2011, 8, 1022-1034.	3.1	9
89	Funnel-like Hexameric Assembly of the Periplasmic Adapter Protein in the Tripartite Multidrug Efflux Pump in Gram-negative Bacteria. Journal of Biological Chemistry, 2011, 286, 17910-17920.	3.4	58
90	Functional Implications of an Intermeshing Cogwheel-like Interaction between TolC and MacA in the Action of Macrolide-specific Efflux Pump MacAB-TolC. Journal of Biological Chemistry, 2011, 286, 13541-13549.	3.4	49

#	Article	IF	CITATIONS
91	Structural basis for the recognition of lysozyme by MliC, a periplasmic lysozyme inhibitor in Gram-negative bacteria. Biochemical and Biophysical Research Communications, 2009, 378, 244-248.	2.1	43
92	Crystal Structure of the Periplasmic Component of a Tripartite Macrolide-Specific Efflux Pump. Journal of Molecular Biology, 2009, 387, 1286-1297.	4.2	111
93	Crystal Structure of the Periplasmic Region of MacB, a Noncanonic ABC Transporter [,] . Biochemistry, 2009, 48, 5218-5225.	2.5	44
94	Identification of Amino Acid Residues in the Catalytic Domain of RNase E Essential for Survival of <i>Escherichia coli</i> : Functional Analysis of DNase I Subdomain. Genetics, 2008, 179, 1871-1879.	2.9	13
95	Calcium-Dependent Catalytic Activity of a Novel Phytase fromBacillus amyloliquefaciensDS11. Biochemistry, 2001, 40, 9669-9676.	2.5	87